Structure and Hydrogen Bonding in Neat *N*-Methylacetamide: Classical Molecular Dynamics and Raman Spectroscopy Studies of a Liquid of Peptidic Fragments†

T. W. Whitfield,‡ G. J. Martyna,*,‡ S. Allison,§ S. P. Bates,§ H. Vass,§ and J. Crain*,‡,§

IBM T. J. Watson Research Center, Yorktown Heights, New York, 10598, and School of Physics, The University of Edinburgh, Mayfield Road, Edinburgh EH9 3JZ, U.K.

Received: June 10, 2005; In Final Form: September 15, 2005

The results of classical molecular dynamics (MD) simulations and Raman spectroscopy studies of neat liquid *N*-methylacetamide (NMA), the simplest model system relevant to the peptides, are reported as a function of temperature and pressure. The MD simulations predict that near ambient conditions, the molecules form a hydrogen bond network consisting primarily of linear chains. Both the links between molecules within the hydrogen-bonded chains and the associations between chains are stabilized by weak methyl-donated "improper" hydrogen bonds. The three-dimensional structural motifs observed in the liquid show some similarity to protein β-sheets. The temperature and pressure dependence of the hydrogen bond network, as probed by the mode frequency of the experimentally determined amide-I Raman band, blue shifts on heating and red shifts under compression, respectively, suggesting weakened and enhanced hydrogen bonding in response to temperature and pressure increases. Disruption of the hydrogen-bonding network is clearly observed in the simulation data as temperature is increased, whereas the improper hydrogen bonding is enhanced under compression to reduce the energetic cost of increasing the packing fraction. Because of the neglect of polarizability in the molecular model, the computed dielectric constant is underestimated compared to the experimental value, indicating that the simulation may underestimate dipolar coupling in the liquid.

I. Introduction

Hydrogen-bonding (H-bonding) interactions are now known to be important in determining the structural properties of proteins. In particular, hydrogen bonding between the carboxyl oxygen and amide hydrogen atoms in the protein backbone help to stabilize the β-sheet and other motifs.[1] An attractive and efficient means of developing general models of hydrogen bonding without directly involving the complexity of macromolecules is to study the properties of simpler mimics and fragments under a range of pressure and temperature conditions.

In this regard, the molecule *N*-methylacetamide (NMA, C_3H_7NO) holds special status as a minimal model of the peptide linkage. It contains a single peptide group (O═C−N−H) terminated by methyl moieties on the carbonyl carbon and on the amino nitrogen. Its internal degrees of freedom and intermolecular bonding are therefore locally similar to those of polypeptide segments. For instance, the relative orientations of the methyl groups correspond to the conventional $\psi(C'-C^{\alpha})$ and $\phi(N-C^{\alpha})$ main-chain dihedrals. The molecule is also capable of forming relatively strong (N−H···O═C) hydrogen bonds as well as much weaker methyl-donated (C−H···O═C) "improper" hydrogen bonds.[2−9] There has been recent speculation as to the role of these improper hydrogen bonds in β-sheet and α-helix stabilization.[10−13] Note, a further distinguishing feature of NMA is that it has one of the highest static dielectric constants of any liquid ($\epsilon_0 \approx 180$ at $T = 30$ °C[14]). The molecular origin of this high ϵ_0 and its steep decline upon heating[15] is assumed to arise from the strongly temperature-dependent, orientational correlations of a molecule that possesses a large intrinsic dipole moment and forms hydrogen bonds.

Previous simulation studies have been performed both on NMA in water at infinite dilution and on neat liquid NMA. The work has been focused on optimization of potential functions[16−20] (including polarizable models[21−23]), comparison between ab initio and empirical predictions for cis−trans isomerization[24,25] in the gas phase and in water solution, hydrogen bonding in water,[24,26] charge polarization effects using QM/MM methods,[27] solid NMA,[28] liquid NMA[29] and isolated molecule[30] vibrational properties, isolated dimers,[8,31,32,33] larger clusters,[34] and other intramolecular properties including the dipole moment.[20]

Miyazawa performed the earliest spectroscopic investigation of the normal modes of NMA and other monosubstituted amides.[35] Since then, NMA has been studied in pure form by several Raman spectroscopic[28] and resonance Raman[36] measurements. Some of these measurements and a discussion of certain controversial mode assignments have been recently reviewed.[37] A very detailed analysis of the amide-I (C═O stretch) band profile[38] has even enabled a number of structural conclusions to be drawn. The identification of three subbands within amide-I, along with measurements of their respective depolarization ratios and noncoincidence parameters have revealed spectroscopic features assignable to oligomeric chains, locally ordered regions and monomeric molecules coexisting in the liquid. However, these spectroscopic data offer only a qualitative picture of the liquid-state structure and are not able to provide quantitative information on the precise nature of the local order nor on the relative populations or size of extended structures. To our knowledge, the spectroscopic measurements reported in the present work are the first to be taken on the pure material under pressure.

Despite this experimental and theoretical activity, there has been relatively little work performed to elucidate the local and medium range structure of neat liquid NMA and its dependence

† Part of the special issue "Michael L. Klein Festschrift".
‡ IBM T. J. Watson Research Center.
§ The University of Edinburgh.

10.1021/jp053140+ CCC: $33.50 © 2006 American Chemical Society
Published on Web 11/04/2005

on temperature and pressure. In addition, molecular simulations can shed light on the connection to liquid structure of spectroscopic features, and macroscopic properties such as the static dielectric constant, $\epsilon_0(T)$. Through detailed analysis, the question of how the structural motifs of liquid NMA relate to those of proteins can also be addressed. Indeed, the recently observed structural richness of hydrogen-bonded networks in methanol−water mixtures[39] suggests that a series of combined experimental and theoretical investigations of NMA, beginning with the neat liquid, can uncover broadly relevant new insights.

To investigate the properties of neat NMA liquid and gain new physical insights into the behavior of an important biochemical mimic, simulation and experimental Raman spectroscopy studies were performed at a variety of pressures and temperatures. The focus of the work is the investigation of (1) local order and hydrogen bond geometry as well as the topology of the extended hydrogen bond network, (2) the role of improper hydrogen bonds in stabilizing the NMA liquid, (3) the behavior of the structure and bonding far from the ambient conditions, and (4) the relationship between the changes in short and intermediate range order to material properties such as the temperature dependence of the static dielectric constant and the Raman spectra.

II. Methods

A. Computational Details. Classical molecular dynamics simulations of liquid NMA were carried out using the PINY_MD software package[40] in conjunction with the CHARMM22 force field.[19] A cubic simulation box containing 256 trans-NMA molecules, periodic boundary conditions and Ewald summation to compute the electrostatic interactions were employed in the calculations.

The molecules were initially set up on a face-centered cubic lattice with random molecular rotations and the bad contacts were annealed out. After an initial equilibration period of 120 ps in the constant-*NVT* ensemble followed by 120 ps in the constant-*NPT* ensemble, respectively, data were collected over a 1 ns simulation for each of four state points ($T = 35$ °C, 100 °C, and 185 °C, all at $P = 1$ bar, and $T = 100$ °C at $P = 3$ kbar). To determine the dielectric constant of the near-ambient liquid, the simulation time was extended to 50 ns. In addition, a 6912 molecule system was studied to explore finite-size effects on the dielectric constant and on the long range order of the hydrogen bond network. The *NVT* ensemble was simulated using the Nosé−Hoover chain canonical dynamics method,[41,42] while the *NPT* ensemble was simulated using the methodology of refs 43 and 42.

The static dielectric constant, $\epsilon_0(T)$, of a neat liquid can be obtained in a number of ways.[44,45] In the present paper, ϵ_0 is computed using linear response theory applied with boundary conditions consistent with the use of Ewald summation and a nonpolarizable potential model, via the mean square fluctuations of the total dipole moment of the sample[46,47]

$$\epsilon_0(T) = 1 + \frac{4\pi}{3Vk_BT}[\langle M^2\rangle - \langle M\rangle^2] \tag{2.1}$$

where

$$M = \sum_{i=1}^{P} q_i \mathbf{r}_i \tag{2.2}$$

and P is the total number of charges in the system and $\mathbf{r}_i$ the position of the ith charge, q_i. Under the CHARMM22 force field, P is the total number of atoms in the simulation box.

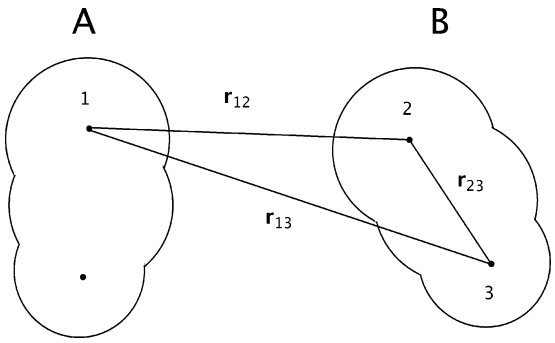

Figure 1. Schematic of a pair of molecules with labeled atomic sites.

Under the CHARMM22 force field, each *trans*-NMA molecule has an average dipole of approximately 4.2 D both in the gas phase and in solution. This value is higher than the 3.73 ± 0.08 D experimental gas-phase dipole,[48] but lower than the approximately 5.2 D predicted using electronic structure calculations for NMA in aqueous solution.[49]

B. Radial and Multidimensional Distribution Functions. It is of general interest to develop structural analysis tools capable of quantitatively probing the intermediate range order in molecular systems. As an elementary example that will subsequently be generalized, consider the standard radial distribution function, $g_{12}(r)$, where r is the radial distance between two atoms, 1 and 2. The radial distribution function is defined such that the average of an operator, $O(r)$, which depends only on the radial distance can be computed as

$$\langle O\rangle = 4\pi\rho\int_0^\infty O(r) r^2 g_{12}(r)\, dr \tag{2.3}$$

Since the fluid achieves its bulk density at large radial distances, in the limit $r \to \infty$ then $g_{12}(r) \to 1$. The coordination number, the number atoms of type 2 in contact with an atom of type 1 at radial distances within the range $\{r_l, r_h\}$, is given by

$$n(\{r_l, r_h\}) = 4\pi\rho\int_{r_l}^{r_h} r^2 g_{12}(r)\, dr \tag{2.4}$$

While simple radial distribution functions show the basic characteristics of a molecular liquid, some of the structural features, particularly those representing intermediate range order, are difficult to characterize using the radial distribution function alone. It is useful, therefore, to extend the radial distribution by considering multidimensional distribution functions between atoms in different molecules. That is, a *joint* distribution with its extra degrees of freedom is capable of distinguishing different conformers, and can help identify important motifs.

To generate useful two-dimensional distribution functions, consider the three atoms in Figure 1: the first atom is taken to reside in molecule "A" while the second and third atoms are both taken to reside in molecule "B". Since atoms 2 and 3 are within molecule B, $\langle|\mathbf{r}_{23}|\rangle$ is well-defined (e.g., atoms are connected via covalent contacts and can never get too far apart. For instance, even a large polymer has a well-defined average end to end distance).

First, the two-dimensional radial distribution function, $g_2(r_{12},r_{13};\bar{f}(r_{23}))$ or for simplicity, $g_2(r,s;q_0)$, where $r = r_{12}$, $s = r_{13}$, and $\bar{f}(r_{23}) = q_0$, is defined such that the average of a quantity, $O(r,s)$, that depends only on the two distances can be written exactly as

$$\langle O\rangle = \left[\frac{2\pi\rho}{q_0}\right]\int_0^\infty \int_0^\infty O(r,s)g_2(r,s;q_0)[rs]\,\mathrm{d}r\,\mathrm{d}s \quad (2.5)$$

where

$$q_0 = [\langle q^{-1}\rangle]^{-1} = \{\int_0^\infty q\,\exp[-\beta\phi_{\mathrm{mf}}(q)]\mathrm{d}q\}^{-1} \quad (2.6)$$

$\phi_{\mathrm{mf}}(q)$ is the potential of mean force upon which q moves, and it is assumed that $q_0 \ll V^{1/3}$. If a strong covalent bond exists between atoms 2 and 3, then $q_0 \approx q_{\mathrm{eq}}$, the equilibrium bond length, a quantity far smaller than the length of the simulation box. In the large r and s limit, the distribution function approaches

$$\lim_{r\to\infty;s\to\infty} g_2(r,s;q_0) = q_0\int_0^\infty q\,\exp[-\beta\phi_{\mathrm{mf}}(q)]\Theta(|r-s|;q)\mathrm{d}q \quad (2.7)$$

where $\Theta(|r-s|;q) = 1$ for $q - |r-s| \geq 0$ and is zero otherwise. When the fluctuations of q are bounded by a strong covalent bond, the limit simplifies to $g_2(r,s;q_0) \approx \Theta(|r-s|;q_0)$ and the distribution function is unity in the restricted domain, $|r-s| \leq q_0 \approx q_{\mathrm{eq}}$. The standard radial distribution functions can be recovered by integration:

$$g(s) = \int_0^\infty g_2(r,s;q_0)\left[\frac{r}{2sq_0}\right]\mathrm{d}r \quad (2.8a)$$

$$g(r) = \int_0^\infty g_2(r,s;q_0)\left[\frac{s}{2rq_0}\right]\mathrm{d}s \quad (2.8b)$$

Note, $g_2(r,s;q_0) \neq g_2(s,r;q_0)$ and $g(s) \neq g(r)$ because atoms 1, 2, and 3 are of different types, with different intermolecular connectivities. The two-dimensional distribution function naturally distinguishes between molecular conformations featuring a short-r contact with a long-s contacts or vice versa as well as cases that possess both short-r and -s contacts.

It is also possible to determine the population or coordination numbers of different types of contacts by integrating the two-dimensional distribution over appropriate limits:

$$n_2(\{r_l,r_h\},\{s_l,s_h\}) = \left[\frac{2\pi\rho}{q_0}\right]\int_{r_l}^{r_h}\int_{s_l}^{s_h} g_2(r,s;q_0)[rs]\,\mathrm{d}r\,\mathrm{d}s \quad (2.9)$$

Similarly, the contribution to the standard distribution function from a particular set of contacts

$$g(s;\{r_l,r_h\}) = \int_{r_l}^{r_h} g_2(r,s;q_0)\left[\frac{r}{2sq_0}\right]\mathrm{d}r \quad (2.10a)$$

$$g(r;\{s_l,s_h\}) = \int_{s_l}^{s_h} g_2(r,s;q_0)\left[\frac{s}{2rq_0}\right]\mathrm{d}s \quad (2.10b)$$

is naturally realized without curve-fitting features in the one-dimensional distribution.

Second, the two-dimensional radial-angular distribution function, $g_2(r_{12},\cos\theta_{123}) \equiv g_2(r,\cos\theta)$ is defined by the radial distance between atoms 1 and 2 and the cosine of the angle formed by the three atoms with atom 2 at the vertex of the triangle. Statistical averages of radial- and angular-dependent quantities are expressed exactly as

$$\langle O\rangle = 2\pi\rho\int_0^\infty \int_{-1}^1 O(r,\cos\theta)g_2(r,\cos\theta)r^2\,\mathrm{d}r\,\mathrm{d}(\cos\theta) \quad (2.11)$$

and $\lim_{r\to\infty} g_2(r,\cos\theta) = 1$. The standard radial distribution is recovered by integration,

$$g(r) = \frac{1}{2}\int_{-1}^1 g_2(r,\cos\theta)\,\mathrm{d}(\cos\theta) \quad (2.12)$$

As above, radial features which arise from different angular correlations can be easily discerned, coordination numbers arising from different angular and radial regions can be obtained, and the contribution to the radial distribution function from different angular features is easily generated without approximation (the latter two quantities require integration over restricted domains, as above). This distribution is useful in hydrogen-bonded systems as it is capable of discerning the angular spread of both proper and improper hydrogen bonds. As an example of a two-dimensional radial−angular distribution function in pure NMA, $g_2(r_{\mathrm{OH}},\cos(\theta_{\mathrm{OHN}}))$ can be defined. As in Figure 1, the oxygen atom is taken to be within molecule A, while the nitrogen and hydrogen atoms are taken to be within molecule B. The angle θ_{OHN} is defined with the hydrogen atom at the vertex. In Figure 2, the θ_{OHN} angle between two hydrogen-bonded NMA dimers is shown.

Finally, consider four atoms: the first and second atoms are taken to reside in molecule A while the third and fourth atoms are both taken to reside in molecule B. Since two pairs of atoms are assumed to lie within the same two molecules, respectively, their distance is bounded (e.g., the pairs of atoms are bounded by covalent contacts). It is useful, therefore, to define a joint distribution function, $g_2(r_{23},\phi_{1234})$, where r_{23} is the distance between atoms 2 and 3 and ϕ_{1234} is the torsion or twist angle between the two planes defined by atoms 123 and 234, respectively. Here,

$$\langle O\rangle = 2\rho\int_0^\infty \int_{-\pi}^\pi O(r,\phi)g_2(r,\phi)\,r^2\,\mathrm{d}r\,\mathrm{d}\phi \quad (2.13)$$

and $\lim_{r\to\infty} g_2(r,\phi) = 1$. The standard radial distribution is recovered by integration:

$$g(r) = \frac{1}{2\pi}\int_{-\pi}^\pi g_2(r,\phi)\,\mathrm{d}\phi \quad (2.14)$$

Coordination numbers and partial distribution functions can be defined in analogy with the previous discussion. The $g_2(r,\phi)$ distribution will clarify the contribution of different molecular twist alignments to various features in the radial distribution function. The azimuthal angle, ϕ, between NMA dimers is drawn in Figure 2. The two special cases of ϕ shown in Figure 2 are refereed to throughout the remainder of this work as "parallel" ($\phi = \pm\pi$) and "antiparallel" ($\phi = 0$).

C. Molecular Cluster Analysis. Using the distribution functions given above, it is possible to define structural criteria—specifically, angular and distance cutoffs—that determine whether two molecules are hydrogen-bonded to one another. This structural definition can then be taken as the basis for defining molecular "chains" or "clusters" of hydrogen-bonded subunits. Hydrogen-bonded molecular chains in liquid NMA have previously been qualitatively identified from Raman spectroscopy.[38] Our simulation data, however, permit the detailed enumeration of hydrogen-bonded chains and the determination of the distribution of chain lengths.

D. Experimental Details. Spectroscopic grade *N*-methylacetamide was obtained from Sigma-Aldrich and used without further purification. A titanium alloy pressure chamber was employed, comprising four horizontal viewing ports at right angles to each other and a vertical polished bore, allowing direct pressurization by top and bottom pistons driven by a hydraulic ram. The port windows are made from low-fluorescence diamonds dry sealed by being lightly clamped in optical contact

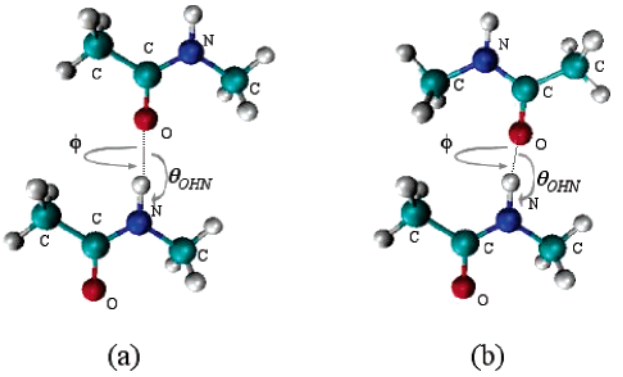

Figure 2. Cartoon structures of hydrogen-bonded *trans*-*N*-methylacetamide dimers. The central peptide linkage is flanked by methyl groups. Strong hydrogen bonding occurs between the amide hydrogen donor and the carbonyl oxygen acceptor and is characterized by an O···H bond length and two independent bond angles, one of which is shown as θ_{OHN} (with the hydrogen atom at the vertex of the triangle OHN). A further degree of freedom is the azimuthal angle, ϕ, about which the hydrogen bond can rotate. Two orientations corresponding to different azimuthal rotations are shown: a "parallel" dimer, with $\phi = \pm\pi$ (a), and "antiparallel" dimer, with $\phi = 0$ (b).

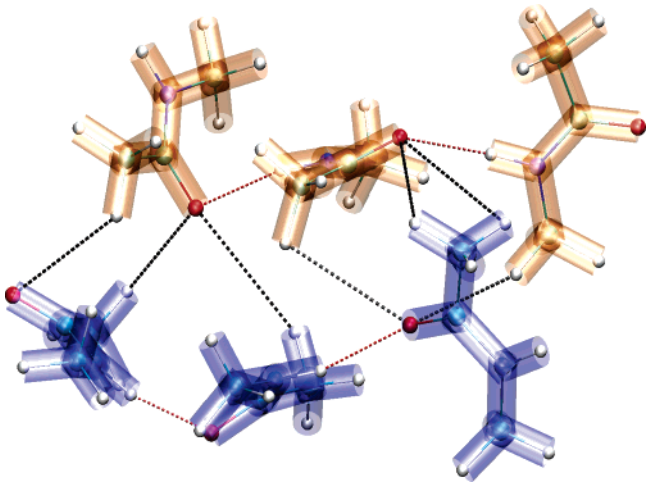

Figure 3. Trimer pair in contact. Each hydrogen-bonded trimer is labeled using a different color. N−H···C═O hydrogen bonds are indicated with dashed red lines while the dashed black lines show the close approach distance between oxygen and methyl hydrogen atoms, all within a 3.2 Å cutoff. These close approaches, taken together with $g(r_{OH_M})$, may imply some stabilization of chain packing by weak methyl-donated (C−H_M···O═C) hydrogen bonds.

to a highly polished surface. This seal gives a negligible contaminant signal and excellent polarization preservation even at high pressure. Heating and temperature control is achieved with heavy-gauge Nichrome wire potted with ceramic cement. Raman spectra are collected in 90°-scattering geometry using the 514.5 nm line (400 mW) of an Ar^+ laser as the exciting line and a Coderg T800 triple-grating spectrometer operating at 1.2 cm^{-1} resolution. A neon emission line was used as an internal frequency standard. Peak frequencies were determined by fitting the Raman spectra to Lorentzian line shapes.

III. Results and Discussion

A. Overview. The results are described in two primary sections. The first section analyzes the liquid structure under near-ambient conditions through the use of several novel metrics applied to the simulation data. The second section explores the structural alterations in the fluid that result from changes in temperature and pressure through a comparison of the results of simulation and experiment.

The structure of the simulated liquid under near-ambient conditions is studied using a variety of complementary approaches, including visualization with molecular graphics, determination of important radial and joint distribution functions, and cluster analysis.

Visualization is essential in order to *qualitatively* assess the liquid structure and identify important structural motifs. Perhaps the single most important structural element visible in the liquid is the existence of chains of hydrogen-bonded NMA molecules. Although hydrogen bonding must therefore be a dominant interaction in determining NMA liquid structure, other interactions, including "improper" hydrogen bonding play a role in the packing of the hydrogen-bonded chains. One structural motif that can be identified visually in liquid NMA—a "sheet" of aligned linear hydrogen-bonded molecular chains that are packed to lie next to one another—is compared with a similar feature in the crystal structure of solid NMA. This sheetlike motif is especially striking when compared with a section of protein β-sheet.

The key elements of liquid NMA structure—hydrogen-bonded chains and interactions between them—is *quantitatively* studied here using radial distribution functions, joint distribution functions and cluster analysis. The multidimensional distribution functions, in particular, allow for the identification of hydrogen-bonded chains that are dimers, trimers, and tetramers and characterize both the linearity of hydrogen bonding and the azimuthal molecular ordering along the chains (see Figure 2). Chains longer than tetrameric have been identified using cluster analysis, and the distribution of chain lengths is reported.

In the second primary section, the temperature and pressure dependence of the hydrogen bond are experimentally addressed using Raman spectroscopy. The results of Raman spectroscopy are supported by comparisons to the structural changes that result from changes in the temperature and pressure in the simulated liquid.

B. Structure under Near-Ambient Conditions. *1. Visualization of the NMA Network Structure.* Visual inspection of the molecular dynamics trajectories using molecular graphics reveals that the liquid is composed of a fluctuating hydrogen bond network of linked polymeric chains. As an example, a pair of hydrogen-bonded trimer chains are shown in Figure 3. In addition to the standard (N−H···O═C) hydrogen bonds that form the two chains shown in Figure 3, there are many "improper" (C−H_M···O═C) hydrogen bond contacts *between* the chains. Improper hydrogen bonds can also be found *within* the hydrogen-bonded NMA chains (for clarity, these are not shown in Figure 3, and NMA molecules within the same hydrogen-bonded trimer chain are indicated with the same color). Given these two types of "improper" hydrogen bonds, it is useful to define the term, "intrachain interaction" to refer to contacts between molecules within the same hydrogen-bonded chain, and the term "interchain interactions" to refer to contacts between molecules belonging to different and distinct hydrogen-bonded chains.

The hydrogen-bonded chains observed in the liquid are roughly linear, and a typical monomer donates and accepts one standard hydrogen bond. The torsion or twist angle (see Figure 2 for a pictorial definition) between two molecules within a hydrogen-bonded chain does not appear to be strongly ordered (for example, in the H-bonded chains of Figures 3 and 4).

It is interesting to note that in some regions of the simulated system, the H-bonded chains are loosely associated into approximately planar sheets as shown in Figure 4. There is a

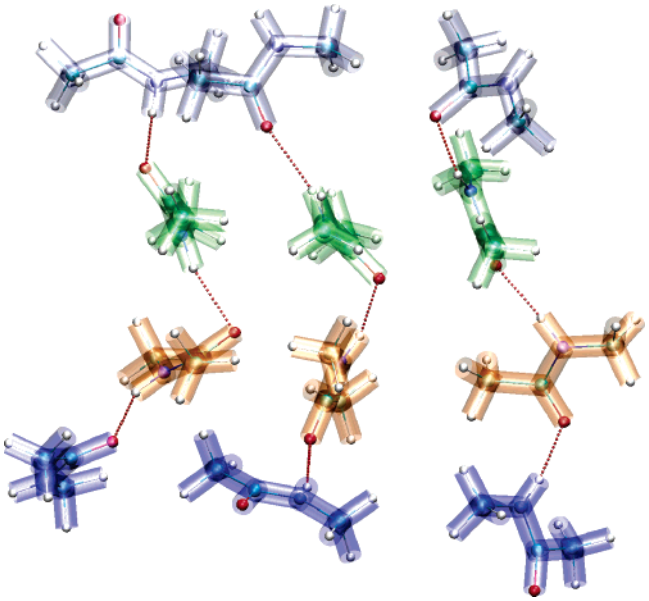

Figure 4. Configuration extracted from a molecular dynamics simulation trajectory of liquid NMA at $T = 35$ °C and $P = 1$ bar. Three hydrogen-bonded chains align to form an approximately planar sheet. The hydrogen bonds in are indicated with dashed red lines. To emphasize the similarities between this structural motif and the β-sheets found in proteins, each of four "strands" in the liquid motif is indicated with a different color. This sheet motif can be compared with the planar sheets in the solid (Figure 6) and a protein β-sheet (Figure 5)

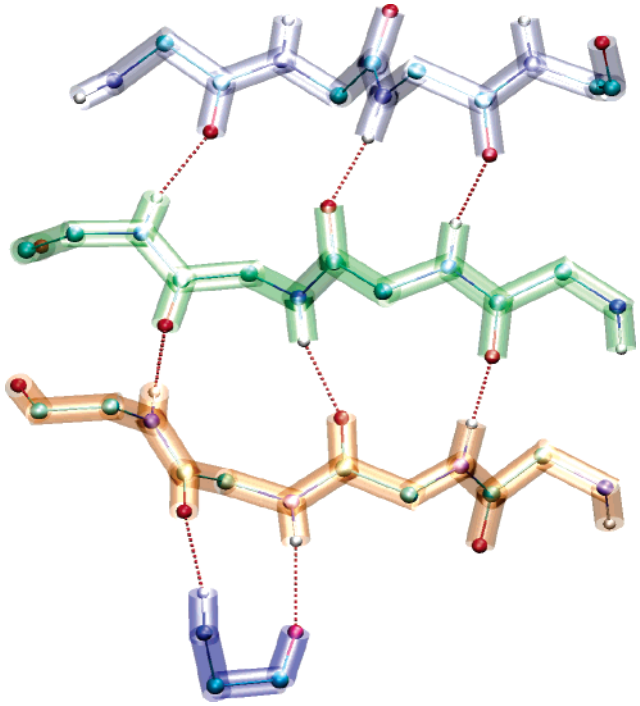

Figure 5. Section of antiparallel protein β-sheet, taken from four of the five strands that form the β-sheet structure of ubiquitin. The strands represented correspond to residues 11−16, 2−7, 66−71, and 41−45. For clarity, only residues 11−14, 4−7, 66−69, and 44 are shown. The coordinates correspond to the solution NMR structure of ubiquitin.[50] Each strand of the β-sheet is labeled with a different color. Hydrogen bonds are indicated with dashed red lines.

reasonable similarity to the hydrogen-bonding motif transverse to polypeptide chains in protein β-sheets given in Figure 5. It can be seen in Figure 5 that a protein β-sheet consists of covalently bonded strands of residues held together in a sheet by hydrogen bonds. The direction of the hydrogen bonding is

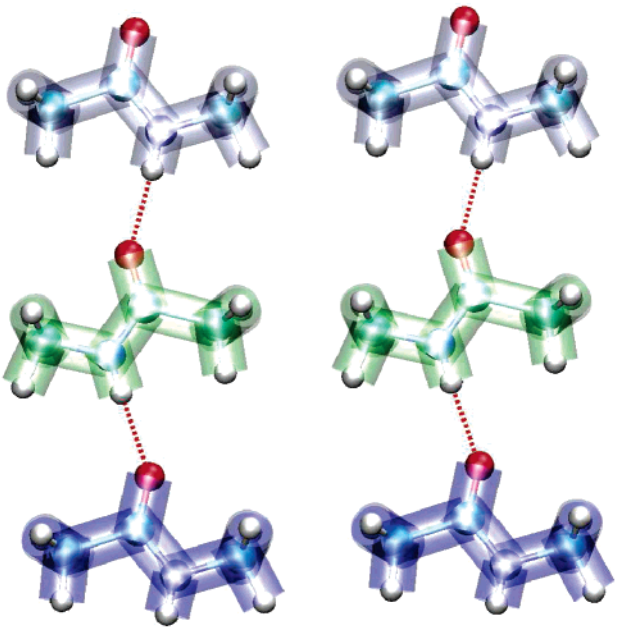

Figure 6. Section of solid NMA.[28,51] In analogy with Figures 4 and 5, molecules that are aligned with one another along the "strand" direction are labeled with like colors. Hydrogen bonds are indicated with dashed red lines.

perpendicular to the direction of the covalent bonds defining the strands. In mapping the NMA liquid structure to the protein, the associated hydrogen-bonded chains are aligned perpendicular to the covalent direction of the protein sheet. Thus, while the strands of the protein β-sheet are held together by strong covalent interactions, the NMA molecules are held together by much weaker interchain interactions, including dipolar couplings and "improper" H-bonds.

To further pursue the analogy to protein β-sheets, note that for any pair of locally aligned hydrogen-bonded chains the relative orientation of the N−H bond direction can be defined. For example, the central four-membered hydrogen-bonded chain in Figure 4 is flanked on the right by a chain of the same N−H bond orientation and by a chain of opposite orientation on the left. By analogy, in both parallel and antiparallel β-sheets, there exists a well-defined N−H bond direction, which alternates between neighboring hydrogen-bonded "chains". This alternation can be observed in Figure 5 (an antiparallel β-sheet). An azimuthal angle, ϕ (see Figure 2), can be defined between neighboring residues along the hydrogen-bonded "chains" in protein β-sheets. In parallel β-sheets, $\phi \approx \pm\pi$ (see Figure 2a), whereas in antiparallel β-sheets $\phi \approx 0$ (see Figure 2b). In contrast, a broad continuous distribution of azimuthal angles is observed in liquid NMA, as will be subsequently shown.

It is also interesting to compare the sheetlike structural motif found in liquid NMA with the structure of crystalline NMA. A planar section of solid NMA is presented in Figure 6. Solid NMA is composed of hydrogen-bonded molecular chains that are aligned with one another and organized into planar sheets (the sheets above and below the section shown in Figure 6 are shifted in the plane of the page in order to efficiently pack). Pairs of NMA molecules that are hydrogen-bonded to one another within the solid are antiparallel $\phi = \pm\pi$. Neighboring molecules from different H-bonded chains are aligned with one another. In some sense, the sheetlike motif of liquid NMA is a remnant of the crystal structure. In the crystal too, improper hydrogen bonds are present—each NMA molecule makes two interchain and one intrachain improper H-bonds.

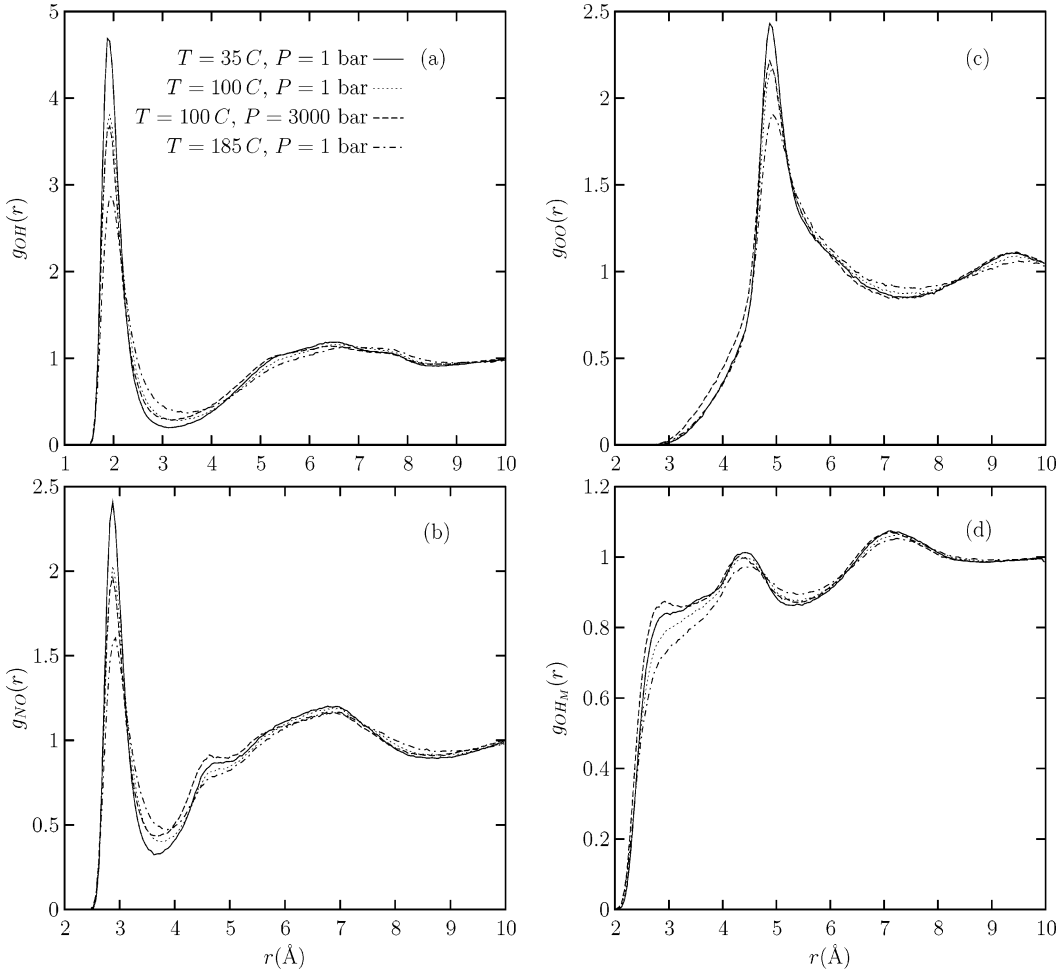

Figure 7. Radial distribution functions for NMA showing the following correlations: (a) $g_{OH}(r)$, (b) $g_{NO}(r)$, (c) $g_{OO}(r)$, and (d) $g_{OH_M}(r)$ (methyl hydrogen). The lines correspond to the state points: $T = 35$ °C (solid line), $T = 100$ °C (dotted line), $T = 185$ °C (dashed−dotted line), all at $P = 1$ bar and $T = 35$ °C, $P = 3.0$ kbar (dashed line). Intramolecular contacts are not shown.

In Figures 4−6, molecules have been color-coded to emphasize the analogy between the liquid NMA sheetlike motif presented in Figure 4 with protein β-sheets, like that presented in Figure 5. Molecules within the same strand are given the same color, so that each of the 4 strands in Figure 5 is colored differently. Similarly, NMA molecules that are part of sheetlike structures in the liquid (Figure 4) and solid (Figure 6) are colored such that molecules in the same strand-like grouping share the same color. The analogy between the sheetlike motif in liquid NMA and protein β-sheets will be further explored in subsequent sections.

Finally, it is useful to discuss the oxygen−oxygen contacts in the structural motifs presented in Figures 4 and 6. If two NMA molecules are linearly hydrogen-bonded to one another, the resulting O−O separation is approximately 5 Å. When hydrogen-bonded chains of NMA associate with one another, as in Figure 4, there are more O−O contacts at a similar (or possibly shorter) separation. These different types of O−O contacts are most easily visualized in solid NMA. The planar section of solid NMA in Figure 6 shows typical O−O contacts for linearly hydrogen-bonded NMA, with $r_{OO} = 4.9$ Å. The closest interchain O−O contacts in the plane of the figure are more distant, at $r_{OO} = 7.2$ Å. Interchain O−O contacts with hydrogen-bonded chains out of the plane in Figure 6 (not shown) are closer, with $r_{OO} = 4.7$ Å.

2. Radial Distributions. While the preceding discussion of the visualization of liquid NMA qualitatively introduces many important structural characteristics, the simulation data permit a detailed quantitative analysis to be performed. Accordingly, a series of radial and joint multidimensional distribution functions are presented below.

The local and intermediate range structural correlations in liquid NMA are represented by selected radial distribution functions shown in Figure 7a−d. To quantitatively identify hydrogen bonds, consider the oxygen-amide hydrogen radial distribution function, $g_{OH}(r)$ (Figure 7a). The first peak is sharp, with a well-defined minimum at $r \approx 3.15$ Å. Integration over this peak gives a coordination number of $n(r = 3.15\ \text{Å}) \approx 0.9$, indicative that each carbonyl oxygen accepts a single hydrogen bond. The $g_{NO}(r)$ distribution (Figure 7b) shows a distinct close contact peak, although there appears to be somewhat more structure between the first and second shells than is typical for simple hydrogen-bonding fluids such as water. The coordination number, integrated to the first minimum of $g_{NO}(r)$ at $r \approx 3.65$ Å, yields $n(r = 3.65\ \text{Å}) = 1.0$.

In contrast to the $g_{OH}(r)$ and $g_{NO}(r)$ distribution functions, the oxygen−oxygen radial distribution function, $g_{OO}(r)$, of Figure 7c, shows unusual features: it has a main peak at $r \approx 4.9$ Å above a high background but also exhibits a long and otherwise featureless tail extending down to much shorter distances ($r \approx 3.0$ Å). The $g_{OO}(r)$ distribution function has a shallow minimum between the first and second maxima. A significant number of oxygen−oxygen contacts must therefore arise for non-hydrogen-bonding molecules, despite the strong correlations that limit the first peaks of the N−O and O−H distributions (as discussed in the preceding section). This

conclusion is supported by the large O−O coordination number: $n(r = 5.5\ \text{Å}) = 5.0$ (in the NMA crystal, $n(r = 5.5\ \text{Å}) = 6.0$).

Weak hydrogen bond-like contacts between carbonyl oxygens and methyl hydrogens, referred to as "improper" hydrogen bonds, have been assigned a secondary role in β-sheet and α-helix stabilization and seem to play a role in determining the properties of NMA (as observed in the preceding section). The distribution of methyl-hydrogen to oxygen contacts, $g_{OH_M}(r)$ (Figure 7d), possesses three main features: a broad shoulder extending from about 3.5 Å down to $r \approx 2.0$ Å, a well-resolved peak just above 4 Å and a broader peak at $r \approx 7.0$ Å. Since most of the methyl hydrogens will not be involved in the improper H-bond-like contacts, it is not surprising that the distribution function is flat. The tail to short distances, however, indicates the existence and structural significance of improper hydrogen bond contacts.

One caveat concerning the improper hydrogen bonds is that a wide variety of $O-H_M$ contact types exist in liquid NMA. This variety is due to the large number of methyl hydrogen sites, the orientational freedom of the molecules and the rotational freedom of the methyl groups themselves. The improper hydrogen-bonded features are therefore "hidden." Note that, in addition to interchain improper H-bonds, it is also possible for methyl-donated improper H-bonds to exist within an (amide hydrogen to carbonyl oxygen) H-bonded NMA dimer. These contacts will also contribute to the low-r intensity in the $g_{OH_M}(r)$ radial distribution function. The other features in this distribution that can be clearly identified include the broad dimer distribution centered near $r = 4$ Å. The peak near $r = 7$ Å is a typical separation between an oxygen atom and a methyl hydrogen in a hydrogen-bonded trimer chain, as shown in Figure 3.

3. Radial and Angular Joint Correlations to Probe Hydrogen Bonding. Using only the standard radial distribution functions presented here, it is difficult to infer which contacts stabilize the complex three-dimensional network structure observed in liquid NMA. To unravel the short and intermediate range order in NMA, it is therefore natural to consider "expanding" the one-dimensional radial distribution functions by introducing two-dimensional joint probability densities in a manner analogous to two-dimensional spectroscopy.

Angular correlations in the (amide) hydrogen bonds can be examined quantitatively by a two-dimensional distribution function $g_2(r_{NO},\cos(\theta_{ONH}))$, which measures the correlation between N−O contact distance against the angular distribution $\cos(\theta_{ONH})$ (see Figure 8). The angle θ_{ONH} is defined with the nitrogen atom at the vertex (see Figure 1). We note that any pair of NMA molecules, A and B, have two pairs of N−O distances, N_A-O_B and N_B-O_A (refer to Figures 1 and 2). If these molecules are members of an approximately linear chain then there always exists one near and one distant N−O contact. The angle convention implies that $\theta_{ONH} \approx 0$ for the near (but not necessarily bonded) contact, whereas $\theta_{ONH} \approx \pm\pi$ for the distant one. With this in mind, the features of Figure 8 can be interpreted as follows: hydrogen-bonded dimers produce the sharply localized feature near $r_{NO} = 3$ Å. As this represents a close contact, we have $\cos(\theta_{ONH})$ centered around 1. In this special case of the close H-bonded pair contact, the angle θ_{ONH} corresponds to the O···H−N hydrogen bond angle. A measure of the H-bond angular disorder is therefore given by the spread on the angular axis and corresponds to $\cos(\theta_{ONH}) \approx \pm 40°$. This H-bond peak is strongly correlated with that at $r_{NO} \approx 6.5$ Å and $\cos(\theta_{ONH}) \approx -1$, which is due to the distant N−O separation in an NMA hydrogen-bonded dimer.

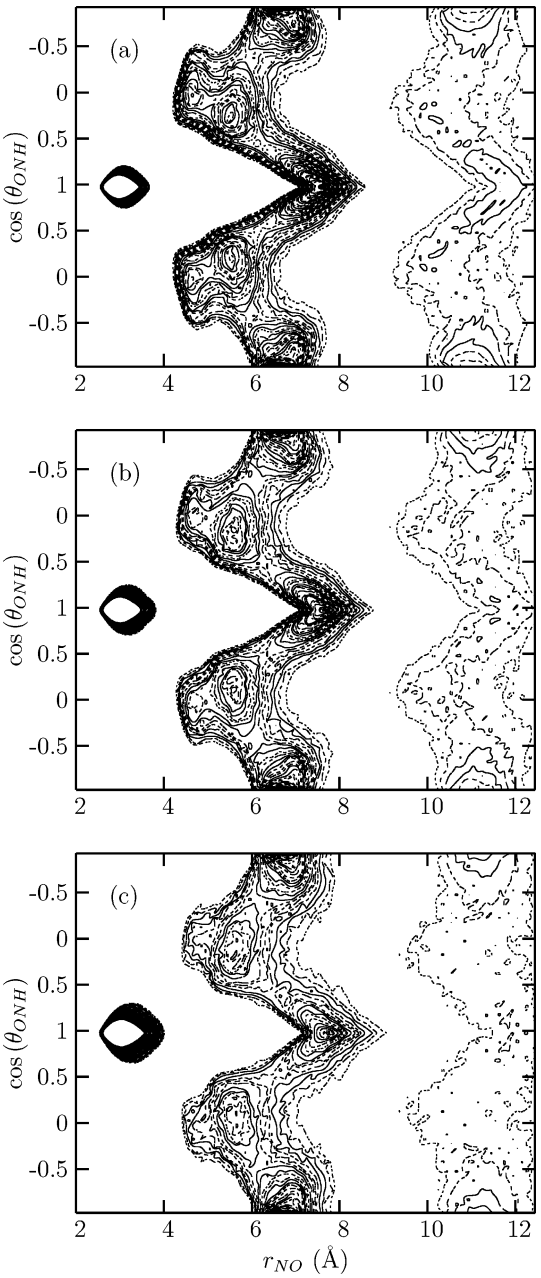

Figure 8. $g_2(r_{NO},\cos(\theta_{ONH}))$ in liquid NMA. The three plots correspond to the temperatures $T = 35$ °C (a), $T = 100$ °C (b), and $T = 185$ °C (c). All are at ambient pressure. The feature at $r_{NO} = 3$ Å and $\cos(\theta_{OHN}) = 1.0$ corresponds to the main hydrogen bond. This peak is directly correlated with that at at $r_{NO} \approx 6.5$ Å and $\cos(\theta_{ONH}) \approx -1$. This second contact represents the longer of the two N−O distances in an NMA dimer.

Although dimer contacts are most prominent, the joint distribution function, $g_2(r_{NO},\cos(\theta_{ONH}))$, allows longer range interactions to be observed. That is, the peak pattern produced by molecules 1 and 3 in a three molecule linear hydrogen-bonded chain should simply mirror that of the dimer features but at an appropriately longer distance. There are two intratrimer contacts visible in Figure 8: the closest appears at $r_{NO} \approx 7.5$ Å and the furthest is responsible for the feature at 11.0 Å. Weak features from the close tetrameric contact are visible at $r_{NO} = 11.5$ Å and $\cos(\theta_{ONH}) \approx 1$. The $g_2(r_{NO},\cos(\theta_{ONH}))$ joint distribution function is therefore a direct probe of intermediate range ordering in liquid NMA.

The majority of the features of the $g_2(r_{NO},\cos(\theta_{ONH}))$ joint distribution can therefore be interpreted on the basis of short and medium-range *intrachain* correlations. An exception is the strong feature spanning the range 4.5 Å $\lesssim r_{NO} \lesssim$ 6.0 Å, which is not easily explained on the basis of isolated hydrogen-bonded chains of NMA molecules. This feature is due primarily to *interchain* associations exhibiting some local orientational preference (see Figures 3 and 4). The presence of this feature is evidence that local chain alignments (which may be stabilized by weak methyl donated improper H-bonds) are common. The duplex−trimer motif given in Figure 3 provides a useful pictorial summary of the main features of the two-dimensional distribution described above

Although the hydrogen-bonded chains present in NMA liquid are clearly important structural elements, the chains contain considerable orientational disorder. Indeed, the joint angular radial distribution, $g_2(r_{OH},\cos(\theta_{HOC}))$, given in Figure 9 demonstrates that a host of structures with angles ranging from 90 to 180° are accessible. The hydrogen-bonding coordination number, defined by integrating the joint distributions, is $n(r_{OH} \in [0,3.15\text{ Å}], \cos(\theta_{HOC}) \in [-0.5,0]) = 0.26$ and $n(r_{OH} \in [0,3.15\text{ Å}], \cos(\theta_{HOC}) \in [-1,-0.5]) = 0.71$ for a total of approximately 1 hydrogen bond. Nonetheless, the large angular spread of $g_2(r_{OH},\cos(\theta_{HOC}))$ at $r = 3.15$ Å indicates that some NMA may be able to accept two (N−H···O═C) hydrogen bonds. This point will be revisited when the cluster analysis results are presented.

The azimuthal angle between hydrogen-bonded dimers (see Figure 2) in the chains can be analyzed using the two-dimensional joint probability distribution function, $g_2(r_{23},\phi_{1234})$, given in eq 2.13. The azimuthal, or twist, angle is defined by the O−H,O−H torsional angle and the distance by the intermolecular separation, r_{OH}. That is, ϕ_{OHOH} is the angle formed between the two planes containing atoms O_A, H_A, O_B and H_A, O_B, H_B, respectively, where the A and B subscripts refer to two distinct molecules (see Figures 1 and 2). This distribution reveals a slight bias toward parallel alignment of dimers, where $\phi_{OHOH} = \pm\pi$ (see Figures 2a and 11). At larger r_{OH} separations, $g_2(r_{OH},\phi_{OHOH})$ reveals a very slight preference for antiparallel alignment of NMA molecules (see Figures 2b and 11). More generally, however, $g_2(r_{OH},\phi_{OHOH})$ points out the high degree of azimuthal angular disorder along hydrogen-bonded chains in liquid NMA.

The azimuthal disorder along the hydrogen-bonded chains in the liquid is in stark contrast with the highly ordered H-bonded chains in crystalline NMA (see Figure 6). In the solid, nearest neighbors within H-bonded chains are perfectly antiparallel ($\phi_{OHOH} = 0$), while next-nearest neighbors are parallel ($\phi_{OHOH} = \pm\pi$), and so on. While the H-bonded chains in the liquid are expected to be more disordered than those found in the solid, it is interesting to note that parallel nearest neighbors are slightly favored in the liquid, compared with antiparallel nearest neighbors in the solid.

Consider the previous analogy with the β-sheet motif of proteins presented in Figures 4 and 5. In this analogy, neighboring hydrogen-bonded chains in liquid NMA can align with one another to form β-sheetlike structures. Liquid NMA "sheets", however, are neither parallel nor antiparallel, due to the large variation permitted in the azimuthal angle. In addition, rather than being covalently bonded (by peptide bonds), as in proteins, the monomers in the liquid "strands" (see Figure 4) are weakly aligned by dipolar intermolecular coupling and by "improper" hydrogen bonds. That is, neighboring molecules within the β-sheetlike motif of liquid NMA are stabilized in the "chain" direction by hydrogen bonds and in the "strand" direction by

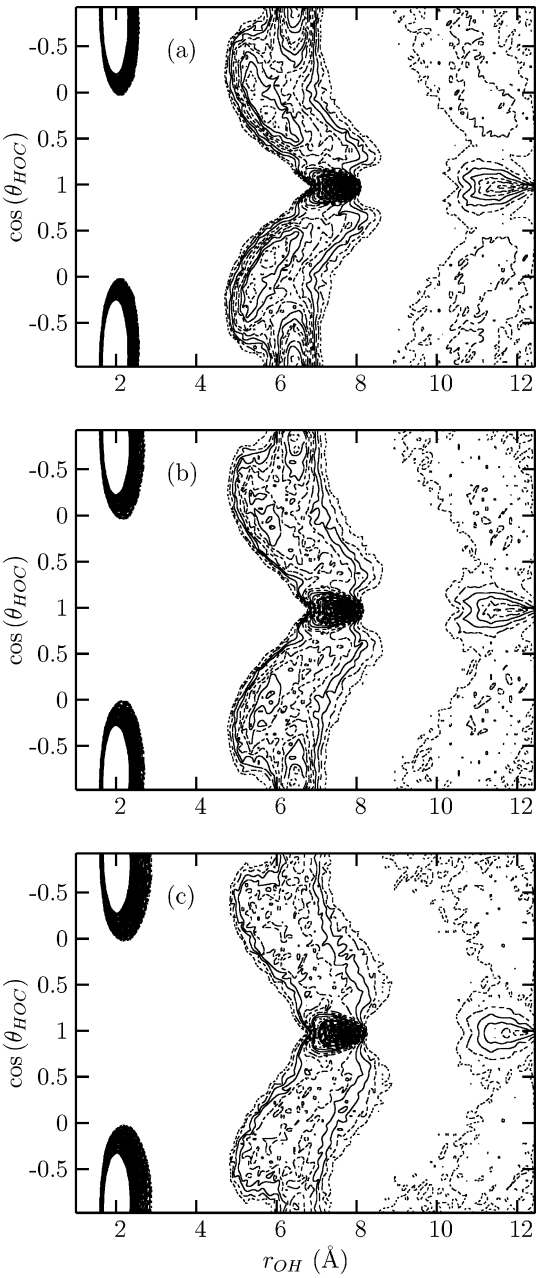

Figure 9. $g_2(r_{OH},\cos(\theta_{HOC}))$ in liquid NMA at three temperatures. The state points in (a−c) are the same as in Figure 8. The angular spread of the feature centered around $r_{OH} = 2$ Å illustrates the level of intrachain orientational disorder.

contacts referred to as interchain interactions throughout this paper. Extending the protein β-sheet analogy to the NMA solid, an antiparallel sheet is observed (see Figure 6). Interchain interactions rigidly align the hydrogen-bonded chains in the NMA crystal.

4. Radial and Angular Joint Correlations to Probe Improper Hydrogen Bonding. Improper hydrogen bonds have been studied, with the goal of separating intra- and interchain contacts. Figure 10 is similar to Figure 9 but with the amide hydrogen atom substituted by a methyl hydrogen atom. The broad feature centered at $r_{OH_M} = 3$ Å and $\cos(\theta_{H_MOC}) = -0.5$, along with that centered at $r_{OH_M} = 6$ Å and $\cos(\theta_{H_MOC}) = 1$, arise from improper hydrogen bonds. The structure in these features is due to the geometry of hydrogen atoms in the methyl groups. The more diffuse contacts visible at larger separations are due to interactions between nonnearest neighbors. In addition to the broadening due to methyl group structure, the joint radial and

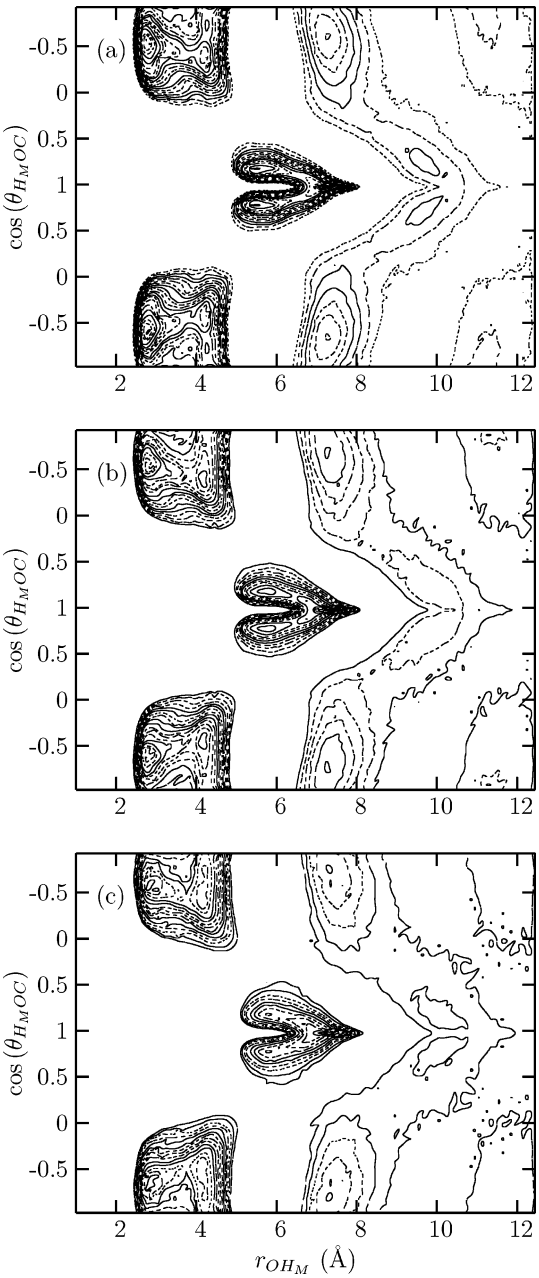

Figure 10. $g_2(r_{OH_M},\cos(\theta_{H_MOC}))$ in liquid NMA at three temperatures. The state points in parts a−c are the same as in Figure 8.

angular distribution functions for improper hydrogen bonding in liquid NMA can also be expected to broaden due to the nondirectional nature of improper hydrogen bonds.[5]

Figure 12 maps the improper hydrogen-bond contacts onto the standard N−H···O═C hydrogen-bond contacts. In addition to intrachain improper H-bond contacts between hydrogen-bonded NMA molecules (with $r_{OH} < 3.2$ Å), there is a peak at approximately $(r_{OH_M},r_{OH}) = (3$ Å,5 Å) corresponding to the type of interchain contacts depicted in Figure 3. Integrating $g_2(r_{OH},r_{OH_M})$ over the intrachain feature gives $n(r_{OH} \in [0,3.2$ Å], $r_{OH_M} \in [0,3.25$ Å]) = 1, or a single improper hydrogen bond. Integrating over the entire feature gives $n(r_{OH} \in [0,3.2$ Å], $r_{OH_M} \in [0,\infty])$ = 6 or all methyl hydrogens of a single hydrogen-bonded NMA molecule. The purely improper (and therefore interchain) hydrogen-bonding feature at $r_{OH} > 3.2$ Å and $r_{OH_M} < 4$ Å integrates to $n(r_{OH} \in [3.2$ Å,$\infty]$, $r_{OH_M} \in [0,2.85$ Å]) = 1 and $n(r_{OH} \in [3.2$ Å,$\infty]$, $r_{OH_M} \in [0,4.0$ Å]) = 6. The interchain improper hydrogen bond contacts are closer than the intrachain contacts.

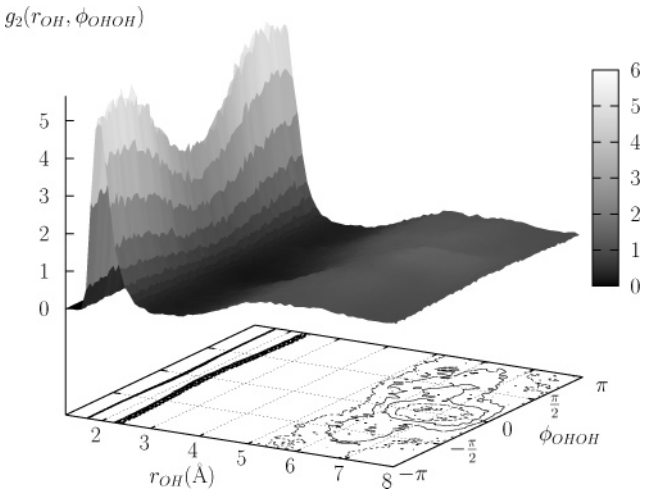

Figure 11. $g_2(r_{OH},\phi_{OHOH})$ in liquid NMA at $T = 35$ °C. $P = 1$ bar.

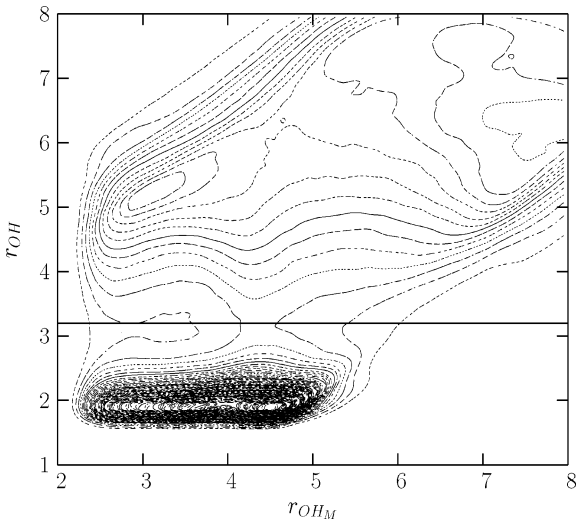

Figure 12. $g_2(r_{OH},r_{OH_M})$ in liquid NMA at $T = 35$ °C. $P = 1$ bar. The r_{OH_M} contacts where $r_{OH} < 3.2$ Å correspond to intradimer contacts.

5. Separating Intra- and Interchain Contacts Involving Oxygen Using a Radial Joint Distribution Function. It has been noted in the preceding sections that interactions between hydrogen-bonded chains, or "interchain" interactions, including improper hydrogen bonds, are important in determining the structure of liquid NMA. Interchain contacts can be invoked to explain the origin of the unusual low-r wing in the oxygen−oxygen radial distribution function, $g_{OO}(r)$, as these contacts cannot arise from pairs of molecules within the same hydrogen-bonded chain.

To quantitatively separate the intra- and interchain contributions to the oxygen−oxygen radial distribution function, the two-dimensional radial distribution, $g_2(r_{OO},r_{ON})$, was constructed (see Figure 13a). In this representation, the hydrogen-bonded peak is observed as a strong feature at $r_{OO} \approx 5$ Å and $r_{NO} \approx 2.85$ Å. The coordination number of the lower quadrant defined by $r_{NO} < 3.75$ Å and $r_{OO} < 5.5$ Å, is n_2(lower left) ≈ 1.0, or a single NMA molecule hydrogen-bonded to the oxygen atom at the origin. The weaker peak at $r_{NO} \approx 6.5$ Å and $r_{OO} \approx 5$ Å is an interchain contact mediated by improper methyl H-bond (see Figure 7d). The coordination number of the upper quadrant defined by $r_{NO} > 3.75$ Å and $r_{OO} < 5.5$ Å is n_2(upper left) ≈ 4. The trimer pair (or "duplex trimer") in Figure 3 shows the two basic O−O contact types: the common intrachain separation (at $r_{OO} = 5.0$ Å) and the closer interchain contact. Overall, the oxygen is "5-fold coordinated" relative to the other oxygens in

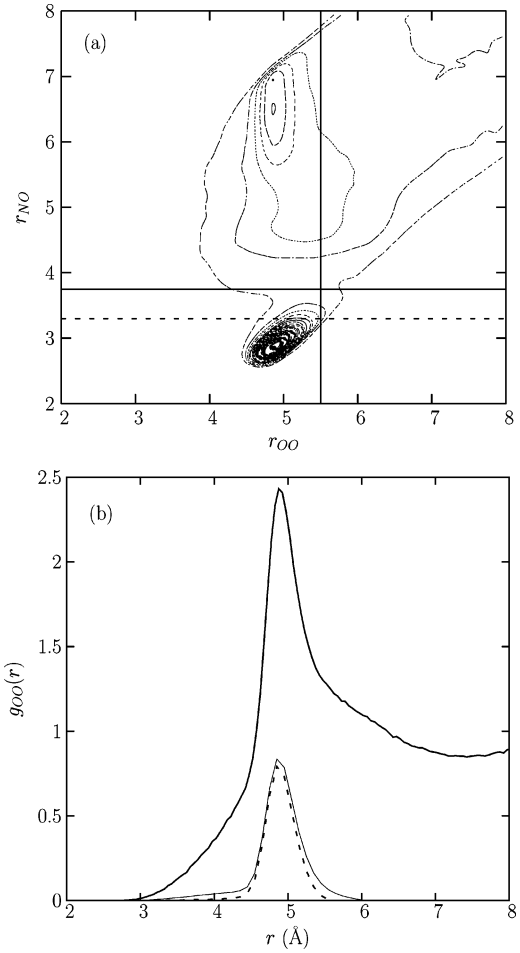

Figure 13. (a) Two-dimensional contact map, $g_2(r_{NO},r_{OO})$, showing the correlation between N−O and O−O distances obtained from averages over the MD trajectories at $T = 35$ °C. The intense peak arises from the intrachain hydrogen bond contact for which the two distances are strongly correlated. Integration over the range $0 \le r_{NO} \le 3.75$ Å extracts $g(r_{OO};r_{NO} \in [0,3.75\ \text{Å}])$, the contribution to $g_{OO}(r)$ arising largely from hydrogen-bonded contacts and is shown in part b. The thin solid curve in part b corresponds to $g(r_{OO};r_{NO} \in [0,3.75\ \text{Å}])$ (see eq 2.10), while the dashed curve is $g(r_{OO};r_{NO} \in [0,3.3\ \text{Å}])$ (the corresponding dashed line is drawn in part a), and the heavy solid curve is the full unrestricted oxygen−oxygen radial distribution.

the system: one strong contact is a nearest NMA neighbor in the same hydrogen-bonded chain and the four weaker diffuse contacts which can drift spatially closer are interchain contacts. Note that there are six oxygen−oxygen contacts with $r_{OO} \approx 5.0$ Å in solid NMA (see Figure 6): two within the hydrogen-bonded chain and four interchain contacts from chains above and below the chain of the central molecule.

The contribution to the $g_{OO}(r)$ distribution function arising only from hydrogen-bonded contacts can be extracted by calculating the restricted distribution $g(r_{OO};r_{NO} \in [0,r_h])$, where r_h is the upper bound on the integration over r_{NO} in eq 2.10. By changing this upper bound, the low-r wing in $g_{OO}(r)$ can be removed. In Figure 13b, the distributions resulting from $r_h = 3.75$ Å and $r_h = 3.3$ Å are both plotted. Although the 3.75 Å cutoff removes most of the wing at small O−O separations, these close contacts are almost entirely eliminated for $r_h = 3.3$ Å.

The closest O−O contacts present in liquid NMA, and explained here as due to contact between NMA molecules that are *not* hydrogen bonded to one another, are not present in solid NMA. The shortest O−O distance *within* the hydrogen-bonded chains (intrachain contact) in solid NMA is $r_{OO} \approx 4.9$ Å, while the shortest O−O distance *between* chains (interchain contact) is $r_{OO} \approx 4.7$ Å. The disorder present in liquid NMA allows for much closer O−O contacts than in the crystal.

6. Cluster Analysis of the Hydrogen-Bonded Network. Loose associations of dimeric, trimeric and tetrameric chain segments have emerged as the structural model that explains the principal features of the radial and angular distribution functions, although twisted filaments of significantly larger size are surely present in this computer model of liquid NMA. The resulting local H-bond pattern exhibits some similarities to that found in the β-sheet motif, albeit with considerably more structural disorder. Furthermore, although visualization of configurations taken from the MD trajectory reveal the presence of much longer H-bonded filaments than tetramers, these longer chains are difficult to see in the two-dimensional distributions due to the average structural disorder beyond the tetrameric length-scale and to the increasingly large volume element (shell) probed at large r. Indeed, these factors account for the asymptotic convergence to unity of the liquid pair and joint distributions. Structural disorder may also make experimental evidence of long filamentary structures difficult to obtain in diffraction experiments—in the only reported (and recent) X-ray diffraction study of liquid NMA,[52] it is suggested that the liquid consists of linear dimers and trimers. It is not clear, however, whether the analysis of the diffraction patterns reported in ref 52 excluded the possibility of chains longer than trimers or whether such structures could not be detected due to the decorrelation induced by thermal disorder.

To make a quantitative characterization of H-bond chain populations present in the simulation studies, membership in an NMA chain based on a structural definition of strong hydrogen-bond connectivity is employed. Specifically, two NMA molecules are assigned as links in the same chain if their intermolecular O−H separation is less than the minimum of the corresponding pair distribution function, $g_{OH}(r)$−about 3.15 Å—and if $\theta_{ONH} \in [0,40°]$ ($\cos(\theta_{ONH}) \in [1,0.766]$; see Figure 8). Averaging over the 1 ns run (during which the hydrogen bond connectivity fluctuates) therefore allows the estimation of relative populations of continuous hydrogen-bonded chains as a function of chain size. The distributions obtained in this way are shown in Figure 14. The distribution of chain lengths for neat liquid NMA are not described by power law behavior at the temperatures studied here, indicating that hydrogen-bonded chains do not percolate throughout the system.

Using our definition of hydrogen bonding, the cluster analysis also reveals that 10% of the molecules are double hydrogen bond acceptors, giving rise to branched H-bonded chains. Hydrogen-bonded rings, however, are not present.

Although there is some sensitivity to the choice of the structural definition chains containing at least 10 members are common. The cumulative probability distribution in Figure 14 (see caption for definition), shows that the probabilities of finding chains containing 10 or more molecules [$1 - \mathbb{P}(9)$] at $T = 35$ °C, $T = 100$ °C and $T = 185$ °C are 0.18, 0.1 and 0.03, respectively. These results are partially consistent with the results from NMR chemical shifts and quantum cluster equilibrium calculations,[34] which anticipated a preference for pentameric hydrogen-bonded chains in liquid NMA. Note that the monomer is the most common individual chain size present in the simulation and there is a steady decay in the probability of occurrence of larger chains.

These conclusions are also broadly consistent with the structural properties inferred from a three-subband decomposition of the amide-I line shape.[38] Specifically, the presence of

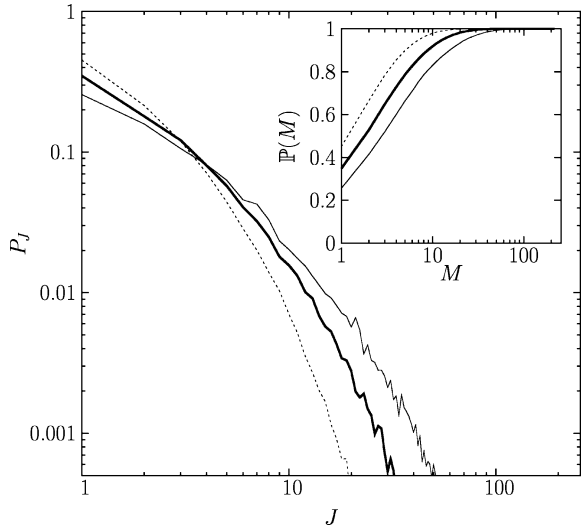

Figure 14. Calculated distribution of hydrogen-bonded chain sizes in liquid NMA at three temperatures (all at $P = 1$ bar): $T = 35$ °C (thin solid line), $T = 100$ °C (bold solid line), and $T = 185$ °C (dashed line). For the purposes of the cluster analysis, two NMA molecules are defined as hydrogen-bonded if the intermolecular O−H contact distance is less than the first minimum in $g_{OH}(r)$ (see Figure 7) and the angular constraint $\theta_{ONH} \in [0,40°]$ ($\cos(\theta_{ONH}) \in [1,0.766]$, see Figure 8). P_J is the probability of finding a hydrogen-bonded NMA chain containing J molecules. Plotted in the inset is the cumulative probability, $\mathbb{P}(M) = \sum_{J=1}^{M} P_J$, of finding a chain containing M or fewer molecules.

monomeric species in the pure material has been inferred from measurements on dilute NMA in acetonitrile. Here it is found that the highest frequency subband within the amide-I envelope increases in intensity on dilution. Its persistence in the pure liquid is evidence for singly occurring NMA molecules. Since a noncoincidence effect (NCE) is not observed for this subband, one assumes that there is no preferential order among monomers.

A noncoincidence effect of about -5 cm^{-1} has been observed for the middle subband of amide-I.[38] This was attributed to some orientational ordering among short oligomers, though it was not possible to determine the nature of the local order as we have done in the present work. The lowest frequency subband has been attributed to longer oligomeric chains. Polarized spectra of this band also show no evidence (from noncoincidence measurements) for preferential alignment of the longer oligomers. The structural data from our simulations, however, clearly indicate that local non-hydrogen-bonded chain contacts are important features of the liquid state.

7. Static Dielectric Constant. A large static dielectric constant is often found in hydrogen-bonded fluids due to the dipolar alignment that is inherent to the network structure of these systems. Indeed, NMA with its strong hydrogen-bonding network (characterized in the preceding section) has one of the highest dielectric constants known for a molecular liquid.

The static dielectric constant (see eq 2.1 for its relation to fluctuations of the system dipole), is known to converge to its asymptotic value slowly in hydrogen-bonded liquids, due to the long relaxation times involved in breaking and forming hydrogen bonds. In view of the rich and complex structure of neat NMA at $T = 35$ *C*, it is not surprising that 50 ns of simulation time are required to generate a good estimate of ϵ_0 via eq 2.1.

The ambient dielectric constant obtained from the simulations under the CHARMM22 force field at $T = 35$ °C is $\epsilon_0 \approx 55 \pm 5$ (see Table 1), an underestimate of the experimental value[14,15] of $\epsilon_0 = 172$. To ensure that there were no finite-size effects in this estimate, simulations were also performed using a 6912-molecule simulation box, yielding a result for ϵ_0 that was consistent with that obtained from the smaller system.

TABLE 1: Static Dielectric Constant for Liquid NMA at Different Temperatures

T (°C)	$\epsilon_0(T)$(expt[a])	$\epsilon_0(T)$
35	172	55 ± 5
100	101	36 ± 5
185	54	26 ± 5

[a] Reference 15.

The origin of the underestimate of the dielectric constant is neglect of the response of the charge distribution of each of the molecules to local environment or many-body (dipole) polarization. Dipole enhancement (relative to gas phase values) occurs when local orientational order creates a Coulomb field and induces a redistribution of the electron density. This property is not contained in the present fixed charge model, although it is evidently significant for NMA.

C. Pressure and Temperature Effects on Structure. The structure of NMA liquid under near-ambient conditions has been analyzed and presented in the preceding sections. In what follows, results are reported from Raman spectra measured over a broad range of experimental temperatures and pressures. Conclusions based upon the Raman spectra are compared with those based upon simulation data taken over the same range of state points. Although it would be ideal to calculate the Raman spectra from the simulation data, such calculations are beyond the scope of the present work.

1. Spectroscopic Survey Far from Ambient Conditions. Hydrogen bonding is accompanied by subtle intramolecular electron charge redistribution and consequently it may have a nonnegligible influence on vibrational frequencies accessible to sufficiently high-resolution optical probes such as Raman spectroscopy. In amides, Raman spectroscopy has proven to be a useful qualitative reporter on structural effects where diffraction data are unavailable—as is currently the case for NMA. In fact, the amide bands of NMA have been studied extensively under ambient conditions and there has been one recent report over the temperature range −196 °C to 100 °C.[53] Particular interest has focused on the region (1200−1700 cm^{-1}) spanning the amide-I, -II, and -III complexes. Of these, the amide-I band (centered at ≈1650 cm^{-1}) is of particular interest and has been most extensively studied in connection with secondary backbone structure in peptides. It is dominated by C═O stretching and includes minor contributions from out-of-phase C−N modes.

In forming an intermolecular H-bond contact between NMA monomers, it is expected that the increasing polarity of the hydrogen bond will deplete electron density from the C═O bond.[53−55] The C═O mode frequency can therefore be used as a qualitative indicator of the strength of hydrogen bonding under various conditions: the hypothesis being that it should red shift when hydrogen bonding increases and blue shift when it diminishes.

The Raman mode frequency corresponding to this amide-I band in liquid NMA is shown as a function of temperature in Figure 15a and as a function of pressure in Figure 15b. It is evident that the band frequency increases with increasing temperature and decreases with increasing pressure. Over the temperature range 36−200 °C, the amide-I mode frequency increases by 20 cm^{-1}. The compression experiments are performed at elevated temperature to inhibit freezing and thereby extend the pressure range. Over the pressure range 1 bar to 5 kbar (at $T = 100$ °C) the amide-I band decreases in frequency by 6 cm^{-1}. This leads to the qualitative conclusion that the

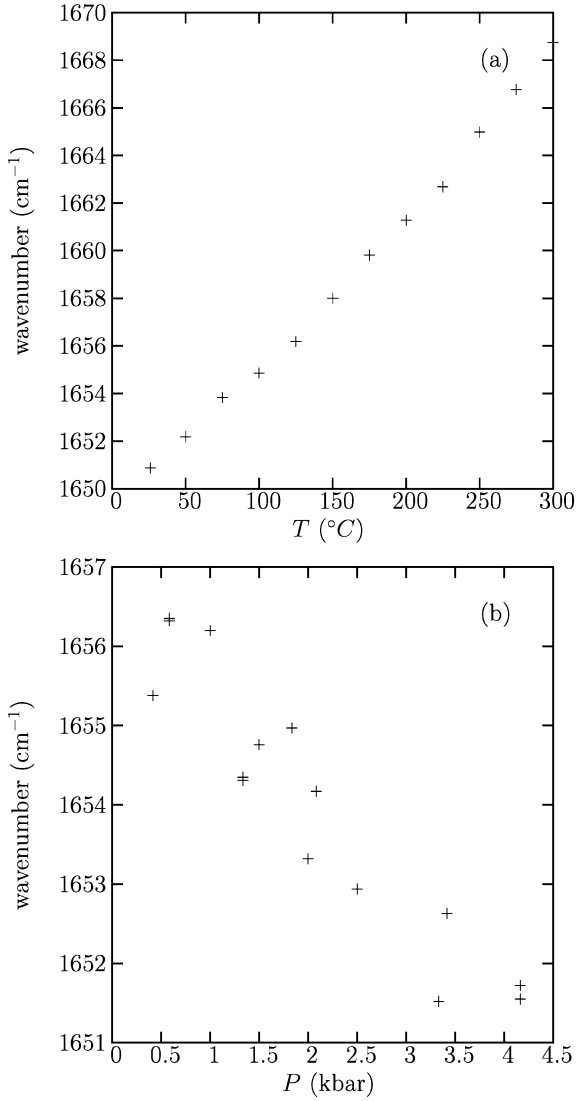

Figure 15. Raman mode frequencies of the amide-I band as a function of temperature (from $T = 36$ °C to $T = 200$ °C) (a) and pressure (from 1 bar to 5 kbar) (b). Pressure measurements made at elevated temperatures ($T = 100$ °C) to avoid freezing of the liquid.

strength of hydrogen bonding decreases on heating and increases under compression. An analysis of the subband behavior of amide-I under pressure has not been carried out because of potential complications with stress birefringence of the diamond windows but will form the basis of further work.

The linear increase of the amide-I band frequency with temperature is well-known behavior though the temperature range over which it is studied here is wider than has been explored before. We know of no other reports of the behavior under compression.

In addition to offering insight into the hydrogen-bonding behavior, a qualitative measure of local ordering can be inferred from the separation between isotropic (polarized) and anisotropic (depolarized) spectra of the amide-I band. In general, the Raman tensor is composed of an (orientation-independent) isotropic component (arising from spherically symmetric average forces) and an orientation-dependent anisotropic component (arising from angular-dependent interactions such as dipole−dipole, higher multipole interactions or hydrogen bonding). The physical origin of this noncoincidence effect (NCE) is thought to be that interactions between the transition dipoles of adjacent molecules affect the isotropic and anisotropic components in different ways in the presence of local ordering.

Experimental separation of the isotropic and anisotropic components and an estimate of the magnitude of the noncoincidence ($\Delta\nu = \nu_{iso} - \nu_{aniso}$) is obtained from polarized Raman spectra in both vertical-vertical and vertical-horizontal scattering geometries ($I_{VV}(\nu)$ and $I_{VH}(\nu)$, respectively). Intensities of the corresponding isotropic and anisotropic bands are thus defined according to

$$I_{aniso}(\nu) = \frac{4}{3} I_{VH}(\nu) \tag{3.1a}$$

$$I_{iso}(\nu) = I_{VV}(\nu) - \frac{4}{3} I_{VH}(\nu) \tag{3.1b}$$

The relationship between the measured NCE and the local ordering in the liquid can be understood in terms of the following perturbation theory expressions:[56,57]

$$\nu_{aniso} = \nu_0 + \frac{1}{2Nm\nu_0} \sum_{\substack{i,j=1 \\ (i \neq j)}}^{N} \langle V_{ij} P_2[\cos(\hat{\mathbf{u}}_i \cdot \hat{\mathbf{u}}_j)] \rangle \tag{3.2a}$$

$$\nu_{iso} = \nu_0 + \frac{1}{2Nm\nu_0} \sum_{\substack{i,j=1 \\ (i \neq j)}}^{N} \langle V_{ij} \rangle \tag{3.2b}$$

where m is the effective mass of the mode (along coordinate Q), N is the number of molecules, and the interaction potential, V_{ij}, is determined by the transition dipole-transition dipole coupling:

$$V_{ij} = \gamma^2 \frac{\hat{\mathbf{u}}_i \cdot \hat{\mathbf{u}}_j - 3(\hat{\mathbf{u}}_i \cdot \hat{\mathbf{n}}_{ij})(\hat{\mathbf{u}}_j \cdot \hat{\mathbf{n}}_{ij})}{R_{ij}^3} \tag{3.3}$$

In the expression for the interaction potential, $\hat{\boldsymbol{u}}_i$ is the unit vector along the transition dipole of molecule i, $\hat{\boldsymbol{n}}_{ij}$ is the unit vector along the line connecting the two oscillators on molecules i and j, $P_2(x)$ is the second-order Legendre polynomial and $\gamma \equiv d\mu/dQ$ is the molecular transition dipole moment.

Since liquids are generally characterized by $|\hat{\boldsymbol{u}}_i \cdot \hat{\boldsymbol{u}}_j| < 1$,[54] it follows that $\Delta\nu$ has the same sign as $\langle V_{ij} \rangle$. Since $\langle V_{ij} \rangle$ is negative for the H-bonded NMA dimer geometry and for short H-bonded molecular chains, these species have been assumed to account for the temperature independent NCE of one of the amide-I subbands in liquid NMA.[38] This assumption implies that dimeric H-bonded contacts persist in liquid NMA over a broad range of temperatures, which is consistent with the calculated distribution of chain lengths presented above. The probability of finding dimers, P_2, is 0.16,0.18 and 0.21, respectively at $T = 36$, 100, and 185 °C. Interestingly, the probability of finding trimers at each of these temperatures, P_3, remains approximately 0.12. The persistence of dimers in liquid NMA over a broad range of temperatures is also confirmed by the structural analysis of the simulations.

In neat NMA liquid under ambient conditions the Raman noncoincidence value was measured to be approximately −6 cm^{-1}. This value is in good agreement with the −5 cm^{-1} value reported in ref 38. We have confirmed that this value is approximately temperature independent up to 120 °C, which is considerably higher than that reported earlier, and suggests that at least dimeric associations persist up to these temperatures.

2. Simulations under Nonambient Conditions. The structural trends in the simulated system are shown in Figure 7a−d. The most significant changes over the temperature range studied occur in the O−H radial distribution function (a) where there

the largest decrease in intensity of the first coordination shell is observed upon heating. We interpret this as an indication that the H-bond connectivity is being broken. Compression up to $P = 3$ kbar makes no visible difference to this distribution. The weak pressure-induced H-bond enhancement indicated by the Raman mode frequency behavior (see Figure 15b) is therefore not discernible in the simulated system from this distribution function.

The effect of pressure on $g_{OO}(r)$ also appears to be small and the main peak position does not shift. However, the small-r tail in the O−O function extends further down to even smaller r in the compressed system. This is due to compression preferentially driving the interchain contacts closer together without significantly compressing the H-bond. In contrast, it is the main peak that is affected more than the low-r wing on heating. This is consistent with the interpretation of the $r = 5$ Å peak as consisting of *both* inter- and intrachain contacts while the low-r intensity arises mainly from interchain contacts. Heating will disrupt the H-bond connectivity (intensity at $r \approx 5$ Å reduced) leaving the nonspecific contacts largely unaltered (low-r wing preserved).

Both pressure and temperature responses of the function g_{OH_M} (Figure 7d) are appreciable at low r, the contributions to which arise from two distinct types of $C-H_M$ contact: one from H-bonded dimers and the other from weak chain-linking H-bonds. As for all distributions, increasing temperature clearly breaks the weak bonds and this is evident here as well. Interestingly, the only nontrivial pressure effect observed in liquid NMA appears in this distribution. A clear enhancement of the $O-H_M$ contact is visible in the low-r region. Specifically, compression of 3 kbar leads to a much more pronounced peak near 3 Å. Since $g_{OH}(r)$ shows negligible pressure response (implying that the H···O−C bond is uncompressed) we conclude that it is the interchain contacts and weak methyl-donated improper hydrogen bonds that are enhanced under pressure as the packing fraction is increased. This enhancement is also consistent with the anomalous high-pressure red shift in the Raman amide-I band.

The effect of heating on the orientational correlations is shown in (b) and (c) of Figures 8−10. Several comments can be made following from the assignments of the main features of these plots.

Consider the $g_2(r_{NO},\cos(\theta_{ONH}))$ distribution in Figure 8. The primary H-bond contact spreads considerably (along both angle and position axes) with increasing temperature; it remains a dominant feature, however. We therefore conclude that dimers with increased H-bond angle disorder persist up to temperatures near boiling. This is also consistent with the qualitative conclusion from the Raman spectroscopic measurements, which showed that the noncoincidence value for liquid NMA has a weak temperature dependence. The features assigned to close and far trimer contacts in Figure 8b and c are greatly reduced for $T = 185$ °C and the close tetramer contact becomes almost unresolvable above the background.

The temperature dependence of the static dielectric constant in the classical model has been studied using eq 2.1. The dielectric data are summarized in Table 1. As expected, $\epsilon_0(T)$ decreases with increasing temperature. Both of the high-temperature values are lower than the experimental results of Lin and Dannhauser,[15] but the underestimate is smaller than the case at the lower temperature of $T = 35$ °C.

IV. Conclusions

The structure and intermediate range order of neat liquid *N*-methylacetamide, a peptidic fragment, have been investigated at a wide range of thermodynamic state points using a combination of high-resolution optical spectroscopy and classical molecular dynamics simulations. The liquid is characterized by polymeric hydrogen-bonded linear and branched chains that can be quite long under near-ambient conditions. Local alignment of trimeric and tetrameric intra- and interchain segments accounts for the main features of the radial and angular distribution functions. The stability of these associations appears to be enhanced by methyl-donated improper hydrogen bonds forming lateral interchain linkages.

The structural motifs therefore show some similarity to the bonding patterns found in β-sheets. It should be emphasized that methyl-donated improper hydrogen bonds have been identified as important as secondary factors in the stabilization of biomolecular complexes including β-sheets and α-helices[8] and in regulating the activity of biological macromolecules.[11] It therefore may be that NMA, in addition to acting as a model system for conventional amide H-bonding, is also a useful prototype for the study of *improper* hydrogen bonds.

The temperature and pressure effects on NMA liquid structure were studied. The disruption of the hydrogen bond chains observed on heating in the simulated system is supported by the experimental blue shift of the amide-I Raman band upon heating. Pressure appears to enhance the weak H-bond contact in order to stabilize an increased packing fraction.

Earlier Raman spectroscopic studies identified the presence of unassociated NMA monomers, aligned dimers and longer oligomeric units in the liquid. These general features are all accounted for in the simulated system and give us confidence in the structural predictions. A number of new and important motifs have been identified, however, via multidimensional distribution functions and from visual inspection of the MD trajectories that had not been inferred from the spectroscopic evidence. These include the presence of very long H-bonded chains, chain branching, improper H-bonds and other motifs that do not have analogues in the NMA crystal structure.

The dielectric constant for all temperatures studied is underestimated by the fixed charged CHARMM22 force field, particularly near ambient temperature. The underestimate is likely caused by the neglect of many-body polarization in the force field. The effect of many-body polarization is greatest at the lower temperatures where stronger local order will lead to larger induced moments.

In summary, the main structural features of neat liquid NMA are dominated by strong hydrogen bonding and will therefore likely be broadly described by the empirical CHARMM22 force field. Definitive tests of the structural predictions will require a combination of neutron diffraction studies, ab initio,[58,59] and path integral[59] molecular dynamics simulations and the development and examination of a polarizable model of NMA, all of which are currently in progress.

Acknowledgment. This work was partly supported by the National Science Foundation grant NSF-0229959 and IBM Research (G.J.M. and T.W.W.), the U.K. Engineering and Physical Sciences Research Council (S.A and J.C.) and Scottish Enterprise (J.C.). T.W.W. would like to thank F. Massi and J.C. would like to thank J. L. Finney, respectively, for helpful discussions.

Note Added after ASAP Publication

This article was released ASAP on November 4, 2005. Equation 3.2a and the text following equation 3.2b has been revised. The correct version was posted on January 26, 2006.

References and Notes

(1) Schulz, G. E.; Schirmer, R. H. *Principles of Protein Structure*; Springer: New York, 1979.

(2) Pimentel, G. C.; McClellan, A. L. *The Hydrogen Bond*; W. H. Freeman and Co.: San Francisco, CA, 1960.

(3) Taylor, R.; Kennard, O. *J. Am. Chem. Soc.* **1982**, *104*, 5063−5070.

(4) Derewenda, Z. S.; Lee, L.; Derewenda, U. *J. Mol. Biol.* **1995**, *252*, 248.

(5) Jeffrey, G. A. *J. Mol. Struct.* **1999**, *485*−*486*, 293−298.

(6) Gu, Y.; Kar, T.; Scheiner, S. *J. Am. Chem. Soc.* **1999**, *121*, 9411−9422.

(7) Vargas, R.; Garza, J.; Dixon, D. A.; Hay, B. P. *J. Am. Chem. Soc.* **2000**, *122*, 4750−4755.

(8) Rossmeisl, J.; Hinnemann, B.; Jacobsen, K. W.; Norskov, J. K.; Olsen, O.; Pedersen, J. *J. Chem. Phys.* **2003**, *118*, 9783.

(9) Manikandan, K.; Ramakumar, S. *Proteins* **2004**, *56*, 768.

(10) Fabiola, G. F.; Krishnaswamy, S.; Nagaragan, V.; Pattabhi, V. *Acta Crystallogr. D* **1997**, *53*, 316−320.

(11) Lei, Y.; Li, H.; Pan, H.; Han, S. *J. Phys. Chem. A* **2003**, *107*, 1574.

(12) Vergenz, R. A.; Yazji, I.; Whittington, C.; Daw, J.; Tran, K. T. *J. Am. Chem. Soc.* **2003**, *125*, 12318−12327.

(13) Zhang, R.; Li, H.; Lei, Y.; Han, S. *J. Phys. Chem. B* **2004**, *108*, 12596.

(14) Leader, G. R.; Gormley, J. F. *J. Am. Chem. Soc.* **1951**, *73*, 5731.

(15) Lin, R.-Y.; Dannhauser, W. *J. Phys. Chem.* **1963**, *67*, 1805.

(16) Jorgensen, W.; Swenson, C. *J. Am. Chem. Soc.* **1985**, *107*, 1489.

(17) Derreumauxa, P.; Vergotenb, G. *J. Chem. Phys.* **1995**, *102*, 8586.

(18) Kaminski, G.; Jorgensen, W. L. *J. Phys. Chem.* **1996**, *100*, 18010.

(19) MacKerell, A. D., Jr.; Bashford, D.; Bellott, M.; Dunbrack, R. L., Jr.; Evanseck, J. D.; Field, M. J.; Fischer, S.; Gao, J.; Guo, H.; Ha, S.; Joseph-McCarthy, D.; Kuchnir, L.; Kuczera, K.; Lau, F. T. K.; Mattos, C.; Michnick, S.; Ngo, T.; Nguyen, D. T.; Prodhom, B.; Reiher, W. E., III; Roux, B.; Schlenkrich, M.; Smith, J. C.; Stote, R.; Straub, J.; Watanabe, M.; Wiórkiewicz-Kuczera, J.; Yin, D.; Karplus, M. *J. Phys. Chem. B* **1998**, *102*, 3586−3616.

(20) Langley, C.; Allinger, N. L. *J. Phys. Chem. A* **2002**, *106*, 5638.

(21) Gao, J.; Pavelites, J. J.; Habibollazadeh, D. *J. Phys. Chem.* **1996**, *100*, 2689.

(22) Iuchi, S.; Morita, A.; Kato, S. *J. Phys. Chem. B* **2002**, *106*, 3466.

(23) Caldwell, J.; Kollman, P. *J. Phys. Chem.* **1995**, *99*, 6208.

(24) Mantz, Y.; Gerard, H.; Iftimie, R.; Martyna, G. *J. Am. Chem. Soc.* **2004**, *126*, 4080.

(25) Wibreg, K.; Rush, D. *J. Org. Chem.* **2002**, *67*, 826.

(26) Guo, H.; Karplus, M. *J. Chem. Phys.* **1992**, *96*, 7273.

(27) Gao, J.; Freindorf, M. *J. Phys. Chem. A* **1997**, *101*, 3182.

(28) Kearley, G. J.; Johnson, M. R.; Plazanet, M.; Suard, E. *J. Chem. Phys.* **2001**, *115*, 2614−2620.

(29) Kwac, K.; Cho, M. *J. Chem. Phys.* **2003**, *119*, 2256.

(30) Gregurick, S.; Chaban, G.; Gerber, R. *J. Phys. Chem. A* **2002**, *106*, 8696.

(31) Langley, C.; Allinger, N. L. *J. Phys. Chem. A* **2003**, *107*, 5208.

(32) Bayly, C. I.; Cieplak, P.; Cornell, W. D.; Kollman, P. A. *J. Phys. Chem.* **1993**, *97*, 10269.

(33) Buck, M.; Karplus, M. *J. Phys. Chem. B* **2001**, *105*, 11000.

(34) Ludwig, R.; Weinhold, F.; Farrar, T. *J. Phys. Chem. A* **1997**, *101*, 8861.

(35) Miyazawa, T.; Shimanouchi, T.; Mizushima, S. *J. Chem. Phys.* **1956**, *24*, 408.

(36) Markham, L.; Hudson, B. *J. Phys. Chem.* **1996**, *100*, 2731.

(37) Schweitzer-Stenner, R. *J. Raman Spectrosc.* **2001**, *32*, 711.

(38) Schweitzer-Stenner, R.; Sieler, G.; Mirkin, N. G.; Krimm, S. *J. Phys. Chem. A* **1998**, *102*, 118−127.

(39) Dougan, L.; Bates, S.; Hargreaves, R.; Fox, J.; Reat, V.; Finney, J.; Soper, A.; Crain, J. *J. Chem. Phys.* **2004**, *121*, 6456.

(40) Samuelson, S.; Martyna, G. *J. Chem. Phys.* **1998**, *109*, 11061.

(41) Martyna, G. J.; Klein, M. L.; Tuckerman, M. *J. Chem. Phys.* **1992**, *97*, 2635−2643.

(42) Martyna, G. J.; Tuckerman, M. E.; Tobias, D. J.; Klein, M. L. *Mol. Phys.* **1996**, *87*, 1117−1157.

(43) Tobias, D. J.; Klein, M. L.; Martyna, G. J. *J. Chem. Phys.* **1994**, *101*, 4177−4189.

(44) Allen, M. P.; Tildesley, D. J. *Computer Simulation of Liquids*; Oxford University Press: Oxford, U.K., 1987.

(45) Heinz, T. N.; van Gunsteren, W. F.; Hunenberger, P. *J. Chem. Phys.* **2001**, *115*, 1125.

(46) Neumann, M.; Steinhauser, O. *Chem. Phys. Lett.* **1983**, *102*, 508.

(47) de Leeuw, S. W.; Perram, J. W.; Smith, E. R. *Annu. Rev. Phys. Chem.* **1986**, *37*, 245.

(48) Weast, R. C., Ed. *Handbook of Chemistry and Physics*, 67th ed.; CRC Press: Boca Raton, FL, 1986−1987.

(49) Gao, J.; Xia, X. *Science* **1992**, *258*, 631.

(50) Cornilescu, G.; Marquardt, J. L.; Ottlger, M.; Bax, A. *J. Am. Chem. Soc.* **1998**, *120*, 6836.

(51) Katz, L.; Post, B. *Acta Crystallogr.* **1960**, *13*, 624.

(52) Trabelsi, S.; Nasr, S. *J. Chem. Phys.* **2004**, *121*, 6380.

(53) Herrebout, W. A.; Clou, K.; Desseyn, H. O. *J. Phys. Chem. A* **2001**, *105*, 4865.

(54) Torii, H.; Tatsumi, M. *J. Chem. Phys.* **1993**, *99*, 8459−8465.

(55) Torii, H.; Tatsumi, T.; Kanazawa, T.; Tasumi, M. *J. Phys. Chem. B* **1998**, *102*, 309−314.

(56) Wang, C. H.; McHale, J. *J. Chem. Phys.* **1980**, *72*, 4039−4044.

(57) McHale, J. *J. Chem. Phys.* **1981**, *75*, 30−35.

(58) Whitfield, T. W.; Martyna, G. J.; Allison, S.; Bates, S. P.; Crain, J. *Chem. Phys. Lett.* **2005**, *414*, 210−214.

(59) Whitfield, T. W.; Crain, J.; Martyna, G. J. *J. Chem. Phys.*, in press.